Computational Materials Science 123 (2016) 121–130

Contents lists available at ScienceDirect

Computational Materials Science

journal homepage: www.elsevier.com/locate/commatsci

First-principles study of vacancy, interstitial, noble gas atom interstitial and vacancy clusters in bcc-W

Gui-Yang Huang [a,*], Niklas Juslin [a], Brian D. Wirth [a,b]

[a] Department of Nuclear Engineering, University of Tennessee, Knoxville, TN, USA
[b] Oak Ridge National Laboratory, Oak Ridge, TN, USA

ARTICLE INFO

Article history:
Received 26 April 2016
Received in revised form 20 June 2016
Accepted 21 June 2016
Available online 2 July 2016

Keywords:
Tungsten
First-principles
Formation energy
Migration energy
Binding energy

ABSTRACT

Based on first-principles calculations, the vacancy and self-interstitial formation energy in bcc-W are 3.19 eV and 9.97 eV. Binding energy between the dumbbell interstitials can be up to 2.29 eV. Binding energy for the first and second nearest neighbor vacancy pair are −0.12 eV and −0.41 eV. The migration barrier of vacancy, He, Ne and Ar interstitial are 1.70 eV, 0.07 eV, 0.15 eV and 0.25 eV. The migration barrier of self-interstitial along ⟨1 1 1⟩ is 0.05 eV. The so-called rotation barrier of self-interstitial is 0.35 eV. The formation energy of He, Ne, Ar substitutional and He, Ne, Ar tetrahedral interstitial are 4.85 eV, 6.42 eV, 9.54 eV and 6.23 eV, 10.40 eV, 15.10 eV, respectively. Binding energy for di-gas atom (He, Ne and Ar) interstitial are 0.95 eV, 2.28 eV and 1.70 eV. The binding energy of noble gas atom interstitial and vacancy cluster are obtained and can be used as an input to build a molecular dynamics (MD) W-Ne potential. Then molecular dynamics (MD) simulations can be used to investigate the mechanism and temperature dependence of the surface modification of plasma-facing tungsten in the application of future fusion reactors in the following investigations.

1. Introduction

Tungsten is a promising candidate material for the divertor in future fusion reactors, due to its high melting temperature, high thermal conductivity and low sputtering erosion. Tungsten has been investigated extensively by first-principles calculations [1–29], including the energetics and kinetics of vacancy and interstitial [2,3,5,7,8,23,26,27], the energetics and kinetics of Helium [6,7,9–12], Ar/Ne/Kr/Xe [28,29], and Hydrogen [10,12,15–18,20,29], Hydrogen and vacancies [10,12,18], and the solute–point defect interactions [19,22]. The interaction of vacancies has been investigated [4,7,8,21], whereas the interaction of self-interstitials in W has not been reported to date. There are still some incompleteness and controversy for the fundamental parameters of bcc-W. We would try to obtain a more complete and more precise set of fundamental parameters and try to resolve the controversies as well.

There is a variation for the ab initio formation energy of vacancy and interstitial at 0 K in the literature, from 3.11 eV to 3.54 eV for vacancy [5,7,9–11,15,19], and from 9.43 eV to 10.42 eV for self-interstitial [5,7,15,21,23]. On the other hand, the experimental vacancy formation energy is 3.5–4.0 eV [32,54–57] at high temperature. No experimental interstitial formation energy is reported.

The ab initio migration barrier of vacancy is from 1.66 eV to 1.78 eV [7,15,21,26]. For the diffusion of self-interstitial, there are some controversies about the ab initio migration barriers, 0.05 eV [5] or 0.004–0.005 eV [14,15,23]. The ab initio rotation barriers of interstitial from one <1 1 1> direction to another <1 1 1> direction is 0.29–0.38 eV [5,8,21,23].

For the ab initio binding energy of divacancy, there are some controversies: attractive interaction or repulsive interaction.

As a divertor material in fusion reactors, tungsten surface will be exposed to a mixed, low energy (10–100 eV) H/He plasma. It was found that during the exposure of a tungsten surface to a low energy mixed H/He plasmas at 1000–2000 K, some low density tendrils (fuzz) would be formed [30]. Such surface modification would affect the surface and erosion properties of the divertor. The mechanism and temperature dependence of the surface modification is still not well understood to date. As known, molecular dynamics (MD) simulations are helpful for investigating such problems, but first require an appropriate interatomic potential, which is built (created) based on a certain functional form and fit to experimental and/or ab initio results. In order to understand the mechanism of "tendrils" formation during the exposure to He plasmas, researchers have exposed the tungsten surface to some other noble gas plasmas [33], but surprisingly no noticeable low density

* Corresponding author.
E-mail addresses: huangguiyang@gmail.com (G.-Y. Huang), njuslin@gmail.com (N. Juslin), bdwirth@utk.edu (B.D. Wirth).

http://dx.doi.org/10.1016/j.commatsci.2016.06.022
0927-0256/

tendrils (fuzz) is found to form. Understanding the difference in bubble formation and surface modification for various different noble gas atoms might help us explain the fuzz. The binding energy of vacancies, He interstitials, He interstitial - tungsten vacancy clusters, etc. are availalbe in the literature [6,7]. For the other noble gas atoms (Ne and Ar), some ab initio data have been reported recently in the literature [28,29]. However, it is still insufficient for the building of W-Ne and W-Ar MD potential. In this paper, we will obtain some of the required parameters by first-principles calculations. Then a W-Ne and W-Ar molecular dynamics (MD) potential is build based on these ab initio results by Backman et al. [65]. Then, atomistic simulations of tungsten surface evolution under low-energy neon implantation are performed to elucidate the role of noble gas in fuzz formation [34].

2. Calculational method and models

The density functional calculations were carried out using the plane-wave based Vienna ab initio simulation package (VASP) [35,36], based on the generalized-gradient approximation (GGA-PBE [37], GGA-PW91 [38,39]). The electron wave functions were described using the projector augmented wave (PAW) method of Blöchl [40] in the implementation of Kresse and Joubert [41]. Plane waves have been included up to 223 eV, 479 eV, 343 eV and 266 eV for pure W, W containing He, W containing Ne, and W containing Ar, respectively. The energy cutoff is set to the maximum energy cutoff of the corresponding systems (to calculate energy difference). That is to say, for different systems, a different energy cutoff is adopted. Electronic states were occupied with a first-order Methfessel-Paxton smearing width of 0.2 eV for most of the calculations. A realspace projection scheme was used for efficient computations for supercell with >20 atoms. Wave function optimization was truncated when the energy difference was less than 1E−5 eV. The optimization procedure was truncated when the residual forces for the relaxed atoms were less than 0.01 eV/Å. For supercell calculations, the shape and volume of the supercell are fixed to the calculated value of perfect supercell or so-called theoretical value. In the literatures, for supercell calculations to investigate point defects, there are two main methods: constant supercell method and volume and/or shape relaxed (fully-relaxed) supercell method. When the used supercell is large enough, both of them would converge to the same results. If the used supercell is not large enough, there will be difference between these two methods. Both methods would induce artificial effects, when the supercell is not large enough. For example, the former would limit the volume relaxation around the point defect, the latter would not limit the volume relaxation around the point defects, but the volume relaxation will be affected by the artificial interaction between periodic images in the supercell. There is controversy about which factors dominate, which may depend on different situations. For VASP, the energy cutoff need to be increased by at least 20% for the volume relaxation method. With the same limit of computer cost, a larger supercell can be adopted for the constant supercell method. We believe the constant supercell method should be better than the fully-relaxed supercell method for large supercell.

Electronic states can be occupied by several different schemes, for metals, mainly by the tetrahedron method with Blöchl corrections (ISMEAR = −5) and Methfessel-Paxton scheme (ISMEAR = 1). The tetrahedron method with Blöchl corrections (ISMEAR = −5) is recommended for the total energy calculations by the VASP software manual. However, the calculated force using ISMEAR = −5 is inaccurate for metals. So the general calculation routine is to first do a calculation using Methfessel-Paxton scheme to optimize (relax) the structure, then do a one step calculation using tetrahedron method with Blöchl corrections to get a precise total energy. However, the k-point converge of the tetrahedron method can be much slower than the Methfessel-Paxton scheme [42] with an appropriate smearing parameter. Since the metal needs numerous k-points to obtain a good convergence, the tetrahedron method is not always better than the Methfessel-Paxton scheme due to the insufficient k-point sampling. For the Methfessel-Paxton scheme, the width of the smearing (SIGMA) must be chosen appropriately. For W, with a 0.1 eV smearing width (SIGMA = 0.1), the Methfessel-Paxton scheme has a similar k-point convergence and similar total energy precision to the tetrahedron method. With enough k-point sampling, a 0.1 eV smearing width is used to avoid the two steps calculations. The default smearing width of 0.2 eV is usually a good choice to compromise the insufficient k-point convergence and artificial contribution of the smearing.

For W, surprisingly, up to a $12 \times 12 \times 12$ k-point sampling is required to obtain a good convergence of formation energy less than 0.01 eV for $4 \times 4 \times 4$, $5 \times 5 \times 5$ and $6 \times 6 \times 6$ supercell. The calculation cost (calculation time and machine memory) is proportional to the number of irreducible k-points. For the configurations with a lower symmetry, the irreducible k-points tend to be too many for the calculations. Due to limitation of computation cost for numerous calculations, a 0.2 eV smearing width, $5 \times 5 \times 5$ k-point and $4 \times 4 \times 4$ supercell are used to obtain the main results, and a 0.1 eV smearing width and $12 \times 12 \times 12$ k-point are used to improve some of the results. It should be mentioned that, all previous reported results for a $4 \times 4 \times 4$ supercell of W in the literatures to date adopted not more than a $5 \times 5 \times 5$ k-point sampling. According to our results, the insufficient k-point sampling can induce at least up to 0.06 eV for the calculated formation energy. For $6 \times 6 \times 6$ supercell, due to computational cost, $3 \times 3 \times 3$ k-points is adopted for the main results (numerous calculations), and $5 \times 5 \times 5$ k-point is used to check and improve some of the results. Specially, in order to obtain precise results for formation energy of vacancy and interstitial, $12 \times 12 \times 12$ and $7 \times 7 \times 7$ k-points are adopted for the $4 \times 4 \times 4$ and $6 \times 6 \times 6$ supercell, respectively.

For the calculations of lattice constant, bulk modulus and elastic constants, due to the small supercell and small computation cost, a sufficient k-point sampling is used, which are not described in detail here. The calculation routine is that to increase the k-point sampling, until the calculated parameters would not change. In addition, due to small computation cost, unnecessary dense k-point sampling has been used to check the results.

For the supercells with $[1,-1,1]$, $[1,1,0]$ and $[-1,1,2]$ basis vectors (the unit cell with $a_1 = 5.49$ Å, $a_2 = 8.97$ Å and $a_3 = 7.77$ Å (PBE)), both $1 \times 3 \times 3$ and $2 \times 6 \times 6$ k-points are used. In order to reveal the interaction of interstitials along $\langle 1\,1\,1 \rangle$ direction, $n \times 1 \times 1$ supercell and $10 \times 2 \times 2$ supercell is used. (n is the number of unit cell along $[1,-1,1]$ direction.) In order to calculate the binding energy of di-interstitial, $5 \times 2 \times 1$ supercell and $1 \times 2 \times 4$ k-points are used. The k-point sampling is limited by the computation cost and purpose.

For the CI-NEB calculations, $5 \times 5 \times 5$ k-point and $4 \times 4 \times 4$ supercell has been used to calculate the migration barrier. For metals, in general, the CI-NEB calculations need much less middle images than semiconductor. Only one image should be sufficient, which have been checked with three images with $3 \times 3 \times 3$ k-point. Using one image can reproduce the reported migration barrier of He in the literature.

3. Basic properties

3.1. Lattice constant

The lattice constant of bcc W is 3.16277 Å and 3.16522 Å at 0 K and 25 °C, respectively [31,44–46]. The calculated and reported

Table 1
Lattice constant of bcc W at 0 K (in Å).

	LDA	PW91	PBE	PBEsol	AM05	Exp.
This work	3.129	3.175	3.171	3.144	3.137	
Reported	3.14 [21] 3.142 [43] 3.14 [24] 3.13 [27]	3.174 [7] 3.175 [11] 3.17 [19] 3.18 [27]	3.171 [10] 3.172 [15] 3.18 [5] 3.19 [21] 3.190 [43] 3.186 [26] 3.17 [27]	3.14 [27]	3.153 [43]	3.163 [44]

Table 3
Formation energy of vacancy in bcc W (in eV).

	LDA	PW91	PBE	PBEsol	AM05	Exp.
This work	3.28	3.05	3.19	3.38	3.52	
Reported	3.27 [21] 3.48 [27]	3.11 [7] 3.16 [11] 3.11 [19] 3.12 [9] 3.18 [27]	3.56 [5] 3.36 [10] 3.34 [15] 3.33 [2] 3.24 [29] 3.21 [21] 3.31 [27]	3.54 [27]	3.54 [21] 3.57 [2]	4.0 ± 0.3 [54] 3.67 ± 0.2 eV [55] 3.76 ± 0.39 [56] 3.6 [32] 3.51 ± 0.2 [57]

lattice constants of bcc W at 0 K are shown in Table 1. Therein PBE produces the best lattice constant, with a 0.0086 Å overestimation. Based on Ref. [31], the lattice constant of bcc W at 3000 K is larger than that at 0 K by up to 0.052 Å.

As-shown in Table 1, the variation of reported lattice constant in the literatures is not large, smaller than 0.02 Å. However, the calculated vacancy formation energy is very sensitive to the lattice constant. For instance, a 0.01 Å increase of lattice constant can induce up to a 0.1 eV increase of vacancy formation energy, which would be shown later. Therefore, the lattice constant should be calculated with a very high precision, which have been performed in this paper. The variation of reported lattice constant can explain part of the variation of reported vacancy formation energy.

3.2. Bulk modulus and elastic constant

The bulk modulus of bcc W at 0 K is 312.24–314.73 GPa [47,48,50]. The calculated and reported bulk modulus of bcc W at 0 K are shown in Table 2. Therein PBE produces the best bulk modulus and elastic constants, with a small underestimation. Due to the small computation cost, they are calculated with a high precision with a fitting scheme. Since both PBEsol and AM05 cannot produce a good lattice constant and bulk modulus, the elastic constants are not calculated, and not shown here.

4. Formation energy of vacancy and interstitial

4.1. Formation energy of vacancy

The experimental vacancy formation energy in bcc W is about 3.6 eV at high temperature [32]. The calculated and reported values are summarized in Table 3. Since the vacancy formation energy using a $3 \times 3 \times 3$ supercell (PW91) is 3.11 eV, larger than that using a $4 \times 4 \times 4$ supercell by 0.06 eV, a $3 \times 3 \times 3$ supercell should be not large enough. When compared with the results of $5 \times 5 \times 5$ and $6 \times 6 \times 6$ supercell, the difference is less than 0.01 eV. That is to say, a $4 \times 4 \times 4$ supercell should be sufficient for the calculation of vacancy formation energy in W. Since the supercell is large enough, the constant supercell method and so-called fully-relaxed supercell method should obtain the same results. Therefore, the variation of reported vacancy formation energy is not due to the adopted supercell method.

Since a 0.01 Å variation of lattice constant can induce up to a 0.1 eV variation of the vacancy formation energy (shown later),

Table 2
Bulk modulus and elastic constants of bcc W at 0 K (in GPa). See the definition of C' and C_{44} in Ref. [47].

	LDA	PW91	PBE	PBEsol	AM05	Exp.
Bulk modulus						
This work	344.33	308.92	311.13	335.77	335.21	
Reported	320 [1] 328 [21] 335 [43] 320 [24] 306.5 [52] 344 [27]	334 [9] 309.9 [49] 310 [27]	296 [21] 310 [43] 294 [24] 304.5 [29] 314 [2] 313 [27]	334 [27]	333 [43] 314.73 [47]	312.24 [48] 314.15 [50] 309.7 [51]
C'						
This work		141.56	147.09			
Reported	174 [1] 155 [21] 166.8 [52]	144.5 [49]	144 [21] 166 [2]			163.80 [50] 164.41 [47] >163.3 [53] 157 [21]
C_{44}						
This work		147.33	152.40			
Reported	149 [1] 170.5 [52]	145.9 [49]	137 [21] 146 [2]			163.13 [50] 163.31 [47] >162.7 [53] 157 [21]

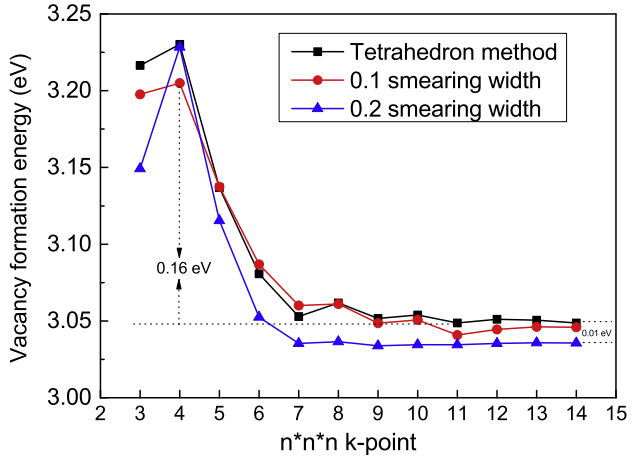

Fig. 1. Vacancy formation energy as a function of $n \times n \times n$ k-point for PW91, using a $4 \times 4 \times 4$ supercell.

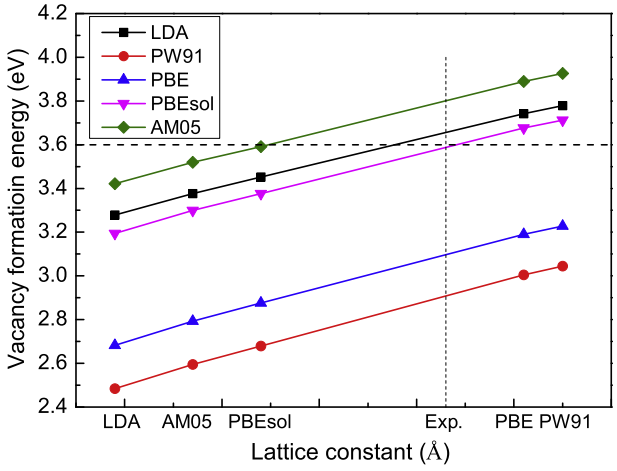

Fig. 2. Vacancy formation energy as a function of lattice constant. The experimental lattice constant at 0 K and experimental vacancy formation energy are also plotted. The corresponding lattice constants are shown in Table 1.

the variation of reported vacancy formation in Table 3 should be partly due to the variation of reported lattice constant. For some of the reported results which adopt almost the same lattice constant as ours, the variation of vacancy formation energy should be due to the insufficient k-point sampling. Vacancy formation energy as a function of $n \times n \times n$ k-point for PW91, using a $4 \times 4 \times 4$ supercell, is shown in Fig. 1. All previous reported results adopted a $3 \times 3 \times 3$, $4 \times 4 \times 4$ or $5 \times 5 \times 5$ k-point sampling. As seen in Fig. 1, previous adopted k-point sampling in the literatures (not more than $5 \times 5 \times 5$ k-point) should be insufficient.

As shown in Table 3, all calculated vacancy formation energies at 0 K in this work are smaller than the experimental value (~3.6 eV). The vacancy formation energy difference between PBE and PW91 is relatively large, up to 0.14 eV, which have been also shown by Medasani et al. [27], up to 0.13 eV. AM05 predicts a closest vacancy formation energy to the experimental value (~3.6 eV), but underestimates the lattice constant by up to 0.03 Å.

The noticeable difference between calculated vacancy formation energy (PBE and PW91) and experimental vacancy formation energy would be analyzed here.

According to Satta et al. [3], vacancy formation energy at experimental temperature may be larger than that at 0 K by up to 0.17 eV due to (formation) electron entropy, based on LDA calculations. It should be mentioned that, the supercell and k-point sampling of Satta et al. [3] may have been insufficient, which predicts a 3.44 eV vacancy formation energy (LDA) at 0 K, and is larger than our results by up to 0.16 eV. In addition, LDA underestimates the lattice constant by up to 0.03 Å (when compared with experiments).

According to Medasani et al. [27], a posteriori surface energy error correction can increase the calculated vacancy formation energy by up to 0.1 eV for LDA, 0.2 eV for PBE, and 0.27 eV for PW91, respectively. If the posteriori surface energy error correction of Medasani et al. [27] is adopted here, the vacancy formation energy of PBE and PW91 are 3.39 eV and 3.32 eV, respectively. If both the (formation) electron entropy [3] and posteriori surface energy error correction [27] are employed, the vacancy formation energy for PBE and PW91 are 3.56 eV and 3.45 eV. The corrected results are close to the experimental value (~3.6 eV). It is unclear whether the (formation) electron entropy correction [3] and posteriori surface energy error correction [27] are valid or not.

The vacancy formation energies as a function of lattice constant, is shown in Fig. 2. The lattice expansion has a strong influence on the vacancy formation energy, and the dependence is relatively insensitive to the choice of functional. An increase of 0.01 Å for lattice constant induces an increase of up to 0.1 eV for calculated vacancy formation energy. Since the experimental vacancy formation energy is measured at high temperature, which should have a larger lattice constant than that at 0 K, it should also have a larger calculated formation energy simply due to the increase of lattice constant (lattice expansion). Based on Ref. [31], the lattice constant of bcc W at 3000 K (3.215 Å) is larger than that at 0 K by about 0.052 Å. Based on a linear extrapolation, the vacancy formation energy at 3000 K should be larger than that at 0 K by up to ~0.5 eV. Since the vacancy formation energy at 0 K based on PBE and PW91 is 3.19 eV and 3.05 eV, respectively, the vacancy formation energy at 3000 K should be about 3.7 eV and 3.6 eV, respectively. The corrected results are close to the experimental value (~3.6 eV). If both the (formation) electron entropy [3] and posteriori surface energy error correction [27] are employed, the vacancy formation energy of PBE and PW91 at high temperature are 3.9 eV and 3.87 eV. Since there exist a relative large variation of experimental vacancy formation energy in Table 3, which result with which correction is the correct one is unclear.

The lattice expansion effect seems to dominate the temperature dependence of the vacancy formation energy, up to ~0.5 eV. The (formation) electron entropy [3] induce about 0.2 eV for the temperature dependence of the vacancy formation energy. If both factors are considered, vacancy formation energy at experimental temperature may be larger than that at 0 K by up to 0.7 eV.

4.2. Formation energy of interstitial

The most stable interstitial in bcc W is the ⟨1 1 1⟩ dumbbell interstitial [5]. The so-called crowdion configuration [5], where five atoms share four lattice sites, is along the ⟨1 1 1⟩ direction rigorously, whereas the ⟨1 1 1⟩ dumbbell interstitial, where two atoms share a lattice site, adopts a tilted configuration [21], where "tilted" means that it is not along the ⟨1 1 1⟩ direction rigorously, and rotates slightly within one of {1 1 0} planes. There are noticeable difference for these two configurations, which the dumbbell interstitial does not simply correspond to the tilted or rotated crowdion interstitial.

The ⟨1 1 1⟩ dumbbell has a 0.052 eV or 0.049 eV lower energy than the ⟨1 1 1⟩ crowdion configuration, based on calculations with a $6 \times 6 \times 6$ supercell ($7 \times 7 \times 7$ k-points) as well as in a supercell with a much longer length along the [1, −1, 1] direction, respectively. Manh et al. [5] and Ventelon et al. [21] have investigated these two configurations, where the tilted ⟨1 1 1⟩ dumbbell is also found to be more stable. Therein the energy difference from Manh

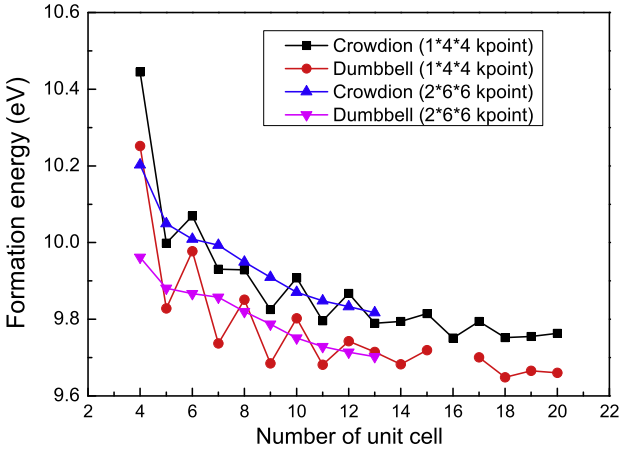

Fig. 3. The formation energy of crowdion and dumbbell interstitial configurations as a function of the number of unit cells along [1,−1,1]. (PBE).

et al. [5] is very small. On the other hand, Ventelon et al. [21] argued that the crowdion configuration is more stable, and that the dumbbell configuration is more stable is only the artificial effect of the long range repulsive interaction along <1 1 1⟩ direction due to an insufficient large supercell. In order to check that, a supercell with [1,−1,1], [1,1,0] and [−1,1,2] basis vectors is used. Based on this type of supercell, the length along [1,−1,1] of the supercell can be increased significantly (with the increase of number of unit cells along that direction). The formation energy of these two interstitial configurations as a function of the number of unit cells along [1,−1,1] is shown in Fig. 3. We can see that, when the interaction along [1,−1,1] is reduced (with the increase of length), the ⟨1 1 1⟩ dumbbell is still more stable than the ⟨1 1 1⟩ crowdion configuration, with a 0.103 eV lower energy. In contrast to the argument of Ventelon et al. [21], the energy difference is more or less insensitive to the long range repulsive interaction along ⟨1 1 1⟩ direction. That is to say, although the long range repulsive interaction along ⟨1 1 1⟩ direction would influence the interstitial formation energy severely, it is similar for both the dumbbell and crowdion configuration, and does not change their relative stability. Therefore, the relative energy difference can be calculated in a reasonable good precision, although there is a long range repulsive interaction along ⟨1 1 1⟩ direction for the used supercell. Although the lateral interaction may be large for the used supercell, it should not change this conclusion, because we focus on when the repulsive interaction along ⟨1 1 1⟩ direction changes, check whether the relative stability of the two interstitial configuration would change as well. If the size of the supercell perpendicular to [1,−1,1] increases twice (with ten unit cells along [1,−1,1]), the calculated energy difference between the dumbbell and crowdion intersitial is 0.049 eV. Thus, combined with the results (0.052 eV) using a $6 \times 6 \times 6$ supercell, we conclude that the dumbbell interstitial has about a 0.05 eV lower energy than the crowndion interstitial. We also used a $5 \times 5 \times 6$ supercell and $5 \times 5 \times 5$ k-points (PBE) to redo the calculations with a non-cubic supercell as mentioned by Ventelon et al. [21], and found that the ⟨1 1 1⟩ dumbbell is still more stable than the ⟨1 1 1⟩ crowdion configuration by 0.076 eV. That is to say, the conclusion of Ventelon et al.[21] that the most stable dumbbell should be along ⟨1 1 1⟩ rigorously is not confirmed and inconsistent with our results. The energy difference between these two configurations is important for the migration barrier of interstitial along ⟨1 1 1⟩ direction, which the corresponding migration barrier should be slightly larger than this energy difference (0.05 eV). The reported calculated migration barrier of 0.004–0.005 eV[14,15,23] should be incorrect. It should be mentioned that the insufficient k-point sampling ($7 \times 7 \times 7$ k-points) may still induce up to 0.01 eV uncertainty for the energy difference.

Table 4
Formation energy of self-interstitial in bcc W (in eV), based on calculations with a $6 \times 6 \times 6$ supercell.

	LDA	PW91	PBE	PBEsol	AM05	Exp.
This work		9.73	9.97	10.52	10.34	
Reported		9.82 [7]	9.55 [5]			9.06 ± 0.63 [58]
		9.43 [23]	10.09 [2]			
			9.86 [15]			
			10.42 [21]			
			10.06 [29]			

In addition, as shown in Fig. 3, there is a long range repulsive interaction between the ⟨1 1 1⟩ interstitial along ⟨1 1 1⟩. Since $6 \times 6 \times 6$ supercell corresponds to 7 unit cells intervals along [1,−1,1], there should still be a large interaction between periodic interstitials for a $6 \times 6 \times 6$ supercell. That is to say, the formation energy of interstitial shown in Table 4 may be noticeably overestimated by up to 0.2 eV.

It should be mentioned that both so-called octahedral and tetrahedral self-interstitial in bcc W have a higher energy than the dumbbell and crowdion configurations [21]. They would not be considered here.

5. Migration barrier of vacancy and interstitial

5.1. Migration barrier of vacancy

According to Mundy et al. [60], the migration barrier of vacancy is 1.68 eV at 1550 K, 1.89 eV at 2200 K and 2.02 eV at 2600 K. According to Satta et al. [3], when extrapolated to 0 K based on a quadratic fit, the migration barrier is 1.5 eV. The calculated and reported values are summarized in Table 5. According to our calculations, when the lattice constant increases by 0.052 Å, the migration barrier tends to decrease by 0.04 eV for PBE (a 1.66 eV migration barrier with a 1.75 Å lattice constant). The trend is opposite to the experimental trend. That is to say, lattice expansion would decrease the migration barrier of vacancy, but not increase the migration barrier of vacancy. The influence of lattice constant on migration barrier is relatively small (0.04 eV), in comparison to the large influence of lattice constant on vacancy formation energy (0.5 eV). It should be mentioned that, since the vacancy formation energy is also dependent on the temperature, the temperature dependence reported by Mundy et al. [60] may be related to the effect of temperature on vacancy formation energy. It seems it should not be assumed that the vacancy formation energy is independent on the temperature.

5.2. Migration barrier of interstitial

It is commonly accepted that the dumbbell self-interstitial diffuses very fast along the ⟨1 1 1⟩ direction. The reported one dimension diffusion along ⟨1 1 1⟩ and rotation barrier are 0.004–0.05 eV [5,14,15,23] and 0.29–0.38 eV [5,8,21–23], respectively. Analytic formula [64] in combination with DFT input is also used to investigate the migration barrier. The correct identification of the most stable dumbbell interstitial is important for the calculation of migration barrier. Since as shown above, the dumbbell interstitial is more stable than the crowdion interstitial by 0.05 eV, the migration barrier of one dimension diffusion along ⟨1 1 1⟩ should

Table 5
Migration barrier of vacancy in bcc W (in eV).

	LDA	PW91	PBE	PBEsol	AM05	Exp.
This work	1.95	1.68	1.70	1.77	1.80	
Reported		1.66 [7]	1.71 [15]			1.7 [59]
			1.78 [21,26]			1.68 ± 0.06 [60]

be at least 0.05 eV. The reported migration barrier of 0.004–0.005 eV [14,15,23] should be incorrect. The reported so-called "soft bending modes" [5,23] should correspond to the transitions between two ⟨1 1 1⟩ dumbbell interstitials along the same ⟨1 1 1⟩ direction. The reported and calculated migration barriers are summarized in Table 6. The calculated rotation barrier and one-dimension barrier along ⟨1 1 1⟩ are 0.35 eV and 0.052 eV (PBE), respectively.

The migration barriers of the noble gas interstitial (He, Ne and Ar) are shown in Table 7. Each of these can diffuse directly from one tetrahedral interstitial site to another. It is unnecessary to go through to the octahedral interstitial. The migration barriers of all three gas atoms are rather small.

In addition, the formation energies of He/Ne/Ar substitutional and interstitial are shown in Table 7. Surprisingly, both the Ne and Ar substitutional formation energy of Manh et al.[29] are close to our corresponding results using PW91, but different from our results using PBE, which has been rechecked carefully. It should be a coincidence. The definition of formation energy is the same as that in the literature.

6. Interaction of vacancies and interstitials

6.1. Interaction of vacancies

The interaction of vacancies has been investigated by Derlet et al. [8], Becquart et al. [7], Muzyk et al. [2], Ventelon et al. [21]

Table 6
Migration barrier of interstitial in bcc W (in eV).

	PW91	PBE
⟨1 1 1⟩	0.056	0.052, 0.05 [5], 0.005 [15], 0.005 [14], 0.004 [23]
Rotation	0.34	0.35,0.29 [5], 0.35 [21], 0.38 [8], 0.347 [23], 0.38 [22]

Table 7
Migration barrier of gas atom interstitial (He, Ne and Ar) and formation energy of gas atom substitutional and interstitial in bcc W (in eV) at 0 K. The reference state of noble gas atom is a single isolated gas atom in vacuum.

Migration barrier	PBE	PW91
He	0.07, 0.07 [29]	0.06 [6], 0.07 [11], 0.06 [28]
Ne	0.15, 0.14 [29]	0.17 [28]
Ar	0.27, 0.23 [29]	0.19 [28]
Formation energy	PBE	PW91
He_{sub}	4.85, 4.83 [29], 5.00 [10]	4.70, 4.70 [6], 4.77 [11]
He_i^{tet}	6.23, 6.22 [29], 6.23 [10]	6.11, 6.16 [6], 6.19 [11], 6.29 [28]
He_i^{oct}	6.48, 6.44 [29], 6.48 [10]	6.35, 6.38 [6], 6.41 [11], 6.67 [28]
Ne_{sub}	6.42, 6.25 [29]	6.21
Ne_i^{tet}	11.40	11.13, 11.55 [28]
Ne_i^{oct}	11.95	11.68, 12.17 [28]
Ar_{sub}	9.54, 9.28 [29]	9.30
Ar_i^{tet}	15.10	14.82, 14.99 [28]
Ar_i^{oct}	16.29	15.97, 16.05 [28]

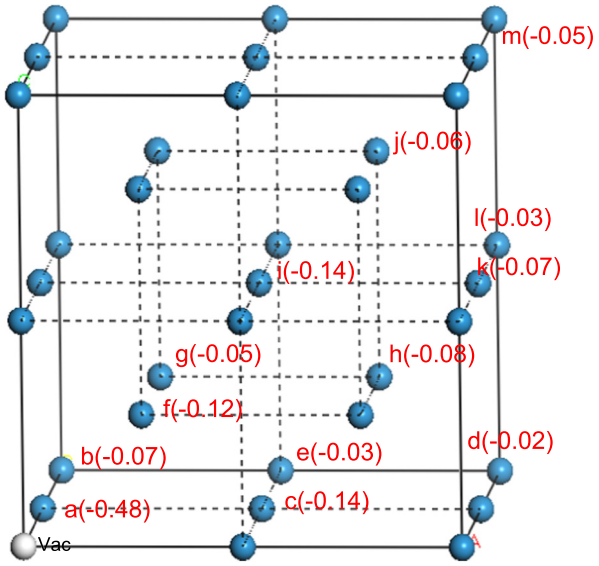

Fig. 4. Binding energy of divacancy. (PBE) The white ball denotes one vacancy of the di-vacancy.

and Oda et al. [26] via first-principles calculations. The binding energy of first nearest neighbor (1NN) and second nearest neighbor (2NN) divacancy pair is 0.41 eV [8], 0.03 eV [2,26], −0.09 eV [21], or −0.12 eV (this work) and 0.19 eV [8], −0.28 eV [26], −0.37 eV [2], −0.41 eV [21], or −0.48 eV (this work) respectively. The definition of binding energy is shown in Ref. [6], not repeated here. Becquart et al. [7] plotted the binding energy but did not show the values. The results of Becquart et al. [7], Ventelon et al. [21] and our calculations are all consistent with each other. The results of Derlet et al. [8] represent an outter. The calculated binding energies of various configurations of divacancy are shown in Fig. 4 (using a $6 \times 6 \times 6$ supecell). We can see that, the binding energy is always negative, which means the interaction between vacancy is always repulsive.

The binding energy of vacancy clusters has been reported by Becquart et al. [61] (Fig. 9 therein) (up to 8 vacancies) and Muzyk et al. [2] (Table 3 and Fig. 12 therein) (up to 6 vacancies). Our calculated results are shown in Fig. 5. Compared with the results of Becquart et al. [61], the binding energies from 2 to 8 vacancies are consistent with each other (PW91). The binding energy

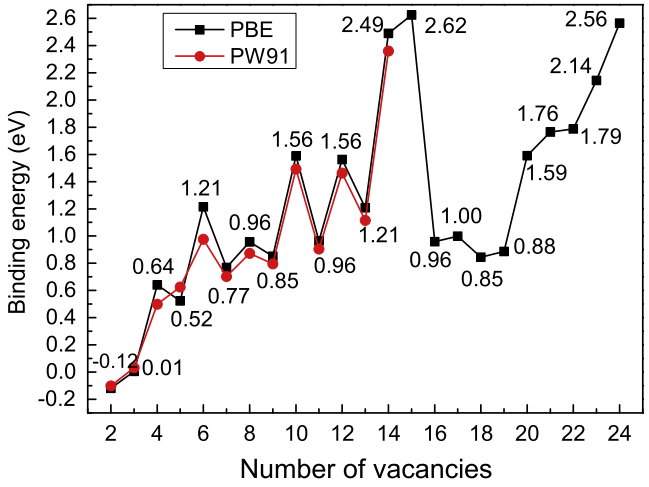

Fig. 5. Binding energy (eV) of one vacancy to a vacancy cluster according to the reaction (m + 1) v + v – >mv. (PBE).

difference between PBE and PW91 is relatively small, but there is still some difference. Therein the values calculated using PBE are also shown in Fig. 5 for convenience. The results of Muzyk et al. [2] are inconsistent with the results of both Becquart et al. [61] and us. It may be due to the insufficient $3 \times 3 \times 3$ k-point sampling in a $4 \times 4 \times 4$ supercell, see Fig. 1.

In addition, we also describe the configurations of the vacancy clusters briefly here for the convenience of theoretical researchers. If someone is not interested in the detail, this section can be skipped. In bcc W, the square (four atoms) and two neighboring body centers (two atoms) forms an octahedron. Two atoms of a line segment of the square, two body centers, and two extra body centers can form another octahedron. Therein the four body centers form a square. These two octahedrons are partially overlapping with each other. It needs only two extra atoms to form a new octahedron. On the other hand, one triangle face (three atoms) of the octahedron and three neighboring atoms can form another octahedron. The new formed octahedron is not overlapping with the original one. It needs three extra atoms to form such an octahedron. For two extra vacancies, it tends to form two partially overlapped octahedrons, whereas, for three extra vacancies, it tends to form two non-overlapped octahedrons. Based on our observations, vacancies tend to form octahedrons, but they tend to form non-overlapped octahedrons, and not partially overlapped octahedrons. When the size of the vacancy cluster increases, sometimes adding an extra vacancy can form a new partially overlapped octahedron. If there are three extra vacancies, they tend to form a non-overlapped octahedron rather than three partially overlapped octahedrons. For two extra vacancies, they tend to form one partially overlapped octahedron rather than two partially overlapped octahedrons. The square (four atoms) and one body center (one atom) forms a pentahedron. Vacancies tend to avoid to form a pentahedron. For five vacancies, they tend to occupy three corners of the square and the two neighboring body centers. For a large size vacancy clusters, a new pentahedron can form together with a new octahedron. For the next added vacancy, it has a strong trend to form a new octahedron to remove the pentahedron. There is a competition between completing an octahedron and avoiding a pentahedron, which is not well checked at present.

6.2. Interaction of interstitials

In order to investigate the interaction of interstitials, we need to know the configuration of interstitial in more detail. The configuration of ⟨1 1 1⟩ dumbbell interstitial has been shown by Manh et al. [5] and Derlet et al. [8], and shown schematically by Ventelon et al. [21] However, the configuration shown by Manh et al. [5] and Derlet et al. [8] is not the most stable configuration, and the configuration shown schematically by Ventelon et al. [21] may cause some misunderstanding. (The dumbbell and crowdion interstitial are not well distinguished.) In order to describe the configuration of interstitial, it is necessary to distinguish the crowdion interstitial and dumbbell interstitial. For the crowdion interstitial, it can be obtained by inserting one extra tungsten atom to the middle of two nearest neighboring atoms along ⟨1 1 1⟩ direction, and relaxing the structure. The inserted atom almost does not change its position, and the neighboring four atoms (two per one side) in the corresponding ⟨1 1 1⟩ direction are pushed away noticeably from the inserted atom, just as shown by Manh et al. [5] and Derlet et al. [8]. The crowdion interstitial has a perfect ⟨1 1 1⟩ symmetry. For the dumbbell interstitial, it can be regarded as a configuration with two atoms sharing one lattice site. The dumbbell does not lie along the ⟨1 1 1⟩ direction rigorously, but rotates slightly within a {1 1 0} plane (without a perfect ⟨1 1 1⟩ symmetry). Based on symmetry considerations, for one ⟨1 1 1⟩ dumbbell, there are three {1 1 0} planes it can rotate within. For a specific {1 1 0} plane, there may

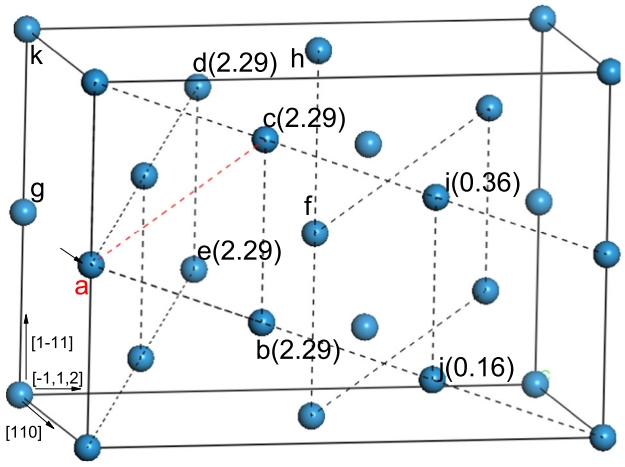

Fig. 6. The structure of bcc W to help understanding the configuration of interstitial and di-interstitial. The value in parentheses are the binding energy of di-interstitial.

be two types of rotations. However, only one of them is stable (the other one will be relaxed to another {1 1 0} plane). The structure of bcc W is shown in Fig. 6. Therein plane (abc) and (ade) are {1 1 0} planes, and plane (afh) and (agk) are symmetric equivalent planes. The atoms in the (1 1 0) plane are not close-packed, where ab < ac, ab and ac correspond to first and second nearest neighboring atom pair, respectively (ac corresponds to the lattice constant of bcc structure). If a dumbbell interstitial is located in site a along [1 −1 1] direction, as shown in Fig. 6, it may rotate slightly towards ab or ac. However, it seems that only the configuration that rotates towards ac within (1 1 0) plane is stable, and that rotates towards ab would be relaxed to another {1 1 0} plane (out of the original (1 1 0) plane). This simplifies the situation, that is to say, there should exist only three configurations for one ⟨1 1 1⟩ direction at one site.

Both the crowdion interstitial and ⟨1 1 1⟩ dumbbell interstitial are very strongly repulsive to each other when they lie in the same ⟨1 1 1⟩ line. When they lie in the different ⟨1 1 1⟩ lines, they tend to attract each other. For the most stable di-interstitial, it corresponds to interstitial pair at ab or ac (with the same binding energy of 2.29 eV). The dumbbell interstitial tends to lie parallel to each other, but due to their interaction, they are not in the (1 1 0) plane, but both rotate slightly within the plane which is perpendicular to the initial (1 1 0) plane. The di-interstitial (ac) can also be completely within one (1 1 0) plane (both of the dumbbell interstitials rotates within that (1 1 0) plane), with a reduced binding energy of 1.67 eV. (The result is not shown in Fig. 6.) Therein dumbbell at a and c rotate towards ab and ac within the (1 1 0) plane, respectively (not parallel to each other). The binding energies for di-interstitial are shown in Fig. 6, where one interstitial locates at site a, and the other interstitial locates at one of the other sites (b, c, d, etc.); the values in the parentheses are the corresponding binding energies. We can see that, there is an relatively short-range attractive interaction perpendicular to the [1 −1 1] direction.

7. Binding energy of noble gas atom-vacancy clusters

7.1. Interaction of He interstitials

The binding energy between two He interstitials in W with various configurations have been calculated by Becquart et al. [6]. The corresponding initial configurations for the di-He interstitial were shown by Becquart et al. [6], which we re-plot in Fig. 7 for the sake of clarity. The denotations of the configurations are the same as those of Becquart et al. [6]. The calculated and reported results are shown in Table 8. The most stable configuration is the

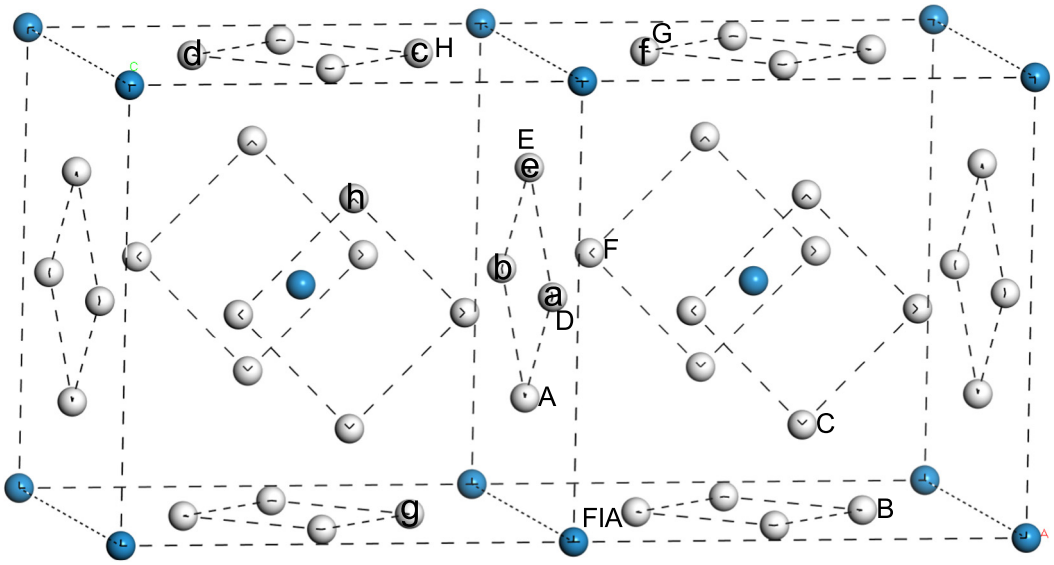

Fig. 7. Schematic configurations of di-He interstitial. The white balls denote potential interstitial sites.

configuration E, consistent with Becquart et al. [6]. Although the initial configurations are the same as those of Becquart et al. [6], some of the relaxed configurations are different, presumably due to the different relaxation step length (we used a very small relaxation step length). For example, the configuration of D and F are exchanged with each other, and the configuration H will relax to configuration E for the results of Becquart et al. [6]. For the most stable configuration E, we used a $6 \times 6 \times 6$ supercell and $5 \times 5 \times 5$ k-point to obtain a better precision. The resulted binding energy is 0.97 eV, similar to the result using a $4 \times 4 \times 4$ supercell and $5 \times 5 \times 5$ k-point (0.95 eV). It indicates that the binding energy of di-He interstitial is relatively insensitive to the supercell size.

Tri-He interstitial (cde), (abe), (bce), (abc) and (acg) have been calculated. (Fig. 7) Tri-He interstitial (acg) will relax to (abc), which is the most stable configuration. For the most stable (abc), c will move towards ab, and stay near the center of the triangle of tungsten atoms (that is to say, within a {1 1 0} plane). We notice that tri-He interstitial tends to stay between two {1 1 0} planes (in an octahedron.).

The most stable four-He interstitial can be obtained by relaxing the configuration with He interstitials in c, d, e and h sites. In fact, the relaxed configuration is related to the most stable tri-He interstitial. The most stable four-He interstitial can be obtained by adding one He interstitial to the neighbor of the tri-He interstitial within the plane determined by the tri-He interstitial. (A new He interstitial triangle is formed.) The four-He interstitials tends to stay between two {1 1 0} planes, and stay almost in a plane. Therein two atoms (the atom corresponding to c and the new added atom) stay almost in another {1 1 0} plane.

The most stable five-He interstitial is not in a single plane, but will not be described here.

The calculated binding energies are shown in Table 9.

7.2. Gas atom-Vacancy cluster

The binding energy between a gas atom-Vacancy cluster and an extra/additional gas atom interstitial are summarized in Tables 9 and 10. We can see that, the noble gas atom (He, Ne and Ar) interstitial has a large binding energy with each other. With the presence (including) of a single vacancy in the cluster, the binding energy between the gas atom-Vacancy cluster and the extra gas atom interstitial increases noticeably. With the increase of gas atoms in the vacancy up to 10, the binding energy only decreases slightly. In fact, even up to 20 gas atoms, the binding energy is not noticeably decreased. Such behaviors are surprising and have been observed for He previously [17,28,63,62], it is also true for Ne and Ar, which may be related to the large binding energy of He/Ne/Ar interstitial without vacancy present. Due to computational cost consideration, only the configurations of He-vacancy clusters are checked in detail, whereas the initial configurations of Ne/Ar-vacancy cluster are obtained based on the ground state of He-vacancy clusters (and several low energy configurations). However, the actual ground state configurations can be different for He, Ne and Ar. According to Tamura et al. [28], the ground state configuration of di-Ne interstitial is different from that of di-He interstitial. If more precise results are needed, further calculations should be needed.

Table 8
Calculated and reported binding energy between two He interstitials (eV).

Position	PBE $4 \times 4 \times 4$ supercell $5 \times 5 \times 5$ kpoint	PBE $6 \times 6 \times 6$ supercell $3 \times 3 \times 3$ kpoint	PW91 [6]
A	0.66	0.64	0.74
B	0.86	0.86	0.94
C	0.94	0.93	1.01
D	0.95	0.93	0.31
E	0.95	0.94	1.03
F	0.25		0.99
G	−0.06	−0.09	−0.04
H	0.04		1.03

Table 9
Binding energy between a He-Vacancy cluster and an additional He interstitials (eV) (PBE).

	0 V	1 V
0He		4.62, 4.57 [7], 4.63 [29]
1He	0.95, 1.03 [6]	3.17, 3.11 [7], 3.10 [29]
2He	1.30, 1.36 [6]	3.14, 3.28 [7], 3.33 [29]
3He	1.61, 1.51 [6]	3.19, 2.61 [7], 3.26 [29]
4He	1.73, 1.64 [6]	2.21, 1.44 [7], 1.88 [29]
5He		2.63, 2.08 [7], 2.18 [29]
6He		2.27
7He		2.45
8He		2.09
9He		2.38

Table 10
Calculated binding energy between a Ne(or Ar)-Vacancy cluster and an additional Ne (or Ar) interstitial (eV) (PBE).

	0 V	1 V		0 V	1 V
0Ne		8.23, 8.18 [29]	0Ar		8.82, 8.54 [29]
1Ne	2.28, 2.72 [28]	4.07	1Ar	1.70, 1.58 [28]	3.58
2Ne	2.79	3.76	2Ar	2.22	3.05
3Ne	3.71	4.89	3Ar	3.72	4.78
4Ne	3.27	4.24	4Ar	2.47	3.15
5Ne	3.21	4.03	5Ar	3.15	2.37
6Ne		4.06	6Ar		3.62
7Ne		4.32	7Ar		4.34
8Ne		4.35	8Ar		3.07
9Ne		4.15	9Ar		3.50

8. Conclusion

We have presented a systematic investigation of the vacancy, interstitial, noble gas atom interstitial and vacancy clusters in W. The purpose is to provide an ab initio data set for the building of a MD potential (W-He, W-Ne, W-Ar, etc.). The main new results are summarized as follows:

1. Calculated vacancy formation energy is smaller than the reported experimental value. Formation electron entropy, surface energy correction, or the effects of lattice expansion appears able to explain the difference.
2. The migration barrier of interstitial along ⟨1 1 1⟩ should be about 0.05 eV. The previously reported 0.004–0.005 eV calculated migration barrier should be incorrect.
3. The binding energy of the most stable di-interstitial is large, up to 2.29 eV. The interaction of the dumbbell interstitials is highly anisotropic. When two dumbbell interstitials locate in one ⟨1 1 1⟩ line, the interaction is repulsive and long-range, whereas, when two dumbbell interstitils locate in different ⟨1 1 1⟩ line, the interaction is attractive and short-range.
4. Single isolated vacancies always tend to repulse each other.
5. The noble gas atoms (He, Ne and Ar) diffuse fast, with a small migration barrier (<0.25 eV).
6. Even without vacancy present, the noble gas atoms in interstitial sites tend to attract each other strongly, with a >0.97 eV binding energy.
7. With a vacancy present (included), the attractive interaction between the noble gas atom interstitial and the cluster increases significantly. The binding energy between the cluster and the gas atom interstitial does not decrease noticeably even when the containing gas atoms increase up to 10.

Acknowledgement

The authors acknowledge partial support for this work from the U.S. Department of Energy Office of Fusion Energy Sciences under grant DOE-DE-SC0006661, and through the Scientific Discovery through Advanced Computing (SciDAC) program on Plasma Surface Interactions, funded by U.S. Department of Energy, Office of Science, Advanced Scientific Computing Research and Fusion Energy Sciences.

References

[1] K. Einarsdotter, B. Sadigh, G. Grimvall, V. Ozolins, Phonon instabilities in fcc and bcc tungsten, Phys. Rev. Lett. 79 (1997) 2073–2076.
[2] M. Muzyk, D. Nguyen-Manh, K.J. Kurzydlowski, N.L. Baluc, S.L. Dudarev, Phase stability, point defects, and elastic properties of W-V and W-Ta alloys, Phys. Rev. B 84 (2011) 104115.
[3] A. Satta, F. Willaime, S. de Gironcoli, Vacancy self-diffusion parameters in tungsten: finite electron-temperature LDA calculations, Phys. Rev. B 57 (1998) 11184.
[4] K.C. Mundim, L.A.C. Malbouisson, S. Dorfman, D. Fuks, J. Van Humbeeck, V. Liubich, Diffusion properties of tungsten from atomistic simulations with ab initio potentials, J. Mol. Struc.-Theochem. 539 (2001) 191–197.
[5] D. Nguyen-Manh, A.P. Horsfield, S.L. Dudarev, Self-interstitial atom defects in bcc transition metals: group-specific trends, Phys. Rev. B 73 (2006) 020101(R).
[6] C.S. Becquart, C. Domain, Migration energy of He in W revisited by ab initio calculations, Phys. Rev. Lett. 97 (2006) 196402.
[7] C.S. Becquart, C. Domain, Ab initio calculations about intrinsic point defects and He in W, Nucl. Instrum. Meth. B 255 (2007) 23.
[8] P.M. Derlet, D. Nguyen-Manh, S.L. Dudarev, Multiscale modeling of crowdion and vacancy defects in body-centered-cubic transition metals, Phys. Rev. B 76 (2007) 054107.
[9] T. Seletskaia, Y. Osetsky, R.E. Stoller, G.M. Stocks, First-principles theory of the energetics of He defects in bcc transition metals, Phys. Rev. B 78 (2008) 134103.
[10] S.C. Lee, J.H. Choi, J.G. Lee, Energetics of He and H atoms with vacancies in tungsten: first-principles approach, J. Nucl. Mater. 383 (2009) 244.
[11] L. Yang, H. Liu, X. Zu, First-principles study of the migration of helium in tungsten, Int. J. Mod. Phys. B 23 (2009) 2077.
[12] C.S. Becquart, C. Domain, An object kinetic Monte Carlo simulation of the dynamics of helium and point defects in tungsten, J. Nucl. Mater. 385 (2009) 223.
[13] C.E. Lekka, N. Bernstein, D.A. Papaconstantopoulos, M.J. Mehl, Properties of bcc metals by tight-binding total energy simulations, Mater. Sci. Eng. B 163 (2009) 8.
[14] T. Ahlgren, K. Heinola, N. Juslin, A. Kuronen, Bond-order potential for point and extended defect simulations in tungsten, J. Appl. Phys. 107 (2010) 033516.
[15] K. Heinola, T. Ahlgren, K. Nordlund, J. Keinonen, Hydrogen interaction with point defects in tungsten, Phys. Rev. B 82 (2010) 094102.
[16] K. Heinola, T. Ahlgren, Diffusion of hydrogen in bcc tungsten studied with first principle calculations, J. Appl. Phys. 107 (2010) 113531.
[17] K. Ohsawa, J. Goto, M. Yamakami, M. Yamaguchi, M. Yagi, Trapping of multiple hydrogen atoms in a tungsten monovacancy from first principles, Phys. Rev. B 82 (2010) 184117.
[18] B. Jiang, F.R. Wan, W.T. Geng, Strong hydrogen trapping at helium in tungsten: density functional theory calculations, Phys. Rev. B 81 (2010) 134112.
[19] Y.L. Liu, H.B. Zhou, Y. Zhang, Investigating behaviors of H in a W single crystal by first-principles: from solubility to interaction with vacancy, J. Alloys Comp. 509 (2011) 8277.
[20] Y.L. Liu, H.B. Zhou, Y. Zhang, G.H. Lu, G.N. Luo, Interaction of C with vacancy in W: a first-principles study, Comp. Mater. Sci. 50 (2011) 3213.
[21] L. Ventelon, F. Willaime, C.C. Fu, M. Heran, I. Gi-noux, Ab initio investigation of radiation defects in tungsten: structure of self-interstitials and specificity of di-vacancies compared to other bcc transition metals, J. Nucl. Mater. 425 (2012) 16.
[22] C.S. Becquart, C. Domain, Solute-point defect interactions in bcc systems: focus on first principles modelling in W and RPV steels, Curr. Opin. Solid State Mater. Sci. 16 (2012) 115.
[23] L. Chen, Y. Liu, H. Zhou, S. Jin, Y. Zhang, G. Lu, Stability and diffusion properties of self-interstitial atoms in tungsten: a first-principles investigation, Sci. China Phys. Mech. Astron. 55 (2012) 614.
[24] S. Giusepponi, M. Celino, The ideal tensile strength of tungsten and tungsten alloys by first-principles calculations, J. Nucl. Mater. 435 (2013) 52.
[25] H.B. Zhou, X. Ou, Y. Zhang, X. Shu, Y.L. Liu, G.H. Lu, Effect of carbon on helium trapping in tungsten: a first-principles investigation, J. Nucl. Mater. 440 (2013) 338.
[26] Y. Oda, A.M. Ito, A. Takayama, H. Nakmura, First-principles study on migration of vacancy in tungsten, Plasma Fusion Res. 9 (2014) 3401117.
[27] B. Medasani, M. Haranczyk, A. Canning, M. Asta, Vacancy formation energies in metals: a comparison of MetaGGA with LDA and GGA exchangeCcorrelation functionals, Comput. Mater. Sci. 101 (2015) 96.
[28] T. Tamura, R. Kobayashi, S. Ogata, A.M. Ito, First-principles investigation of possible clustering of noble gas atoms implanted in bcc tungsten, Model. Simul. Mater. Sci. Eng. 22 (2014) 015002.
[29] Duc Nguyen-Manh, S.L. Dudarev, Trapping of He clusters by inert-gas impurities in tungsten: first-principles predictions and experimental validation, Nucl. Instrum. Meth. Phys. Res. B 352 (2015) 86.
[30] N. Juslin, B.D. Wirth, Interatomic potentials for simulation of He bubble formation in W, J. Nucl. Mater. 432 (2013) 61.
[31] I.K. Suh, H. Ohta, Y. Waseda, High-temperature thermal expansion of six metallic elements measured by dilatation method and X-ray diffraction, J. Mater. Sci. 23 (1988) 757.
[32] J.Y. Park, H.C.W. Huang, R.W. Siegel, R.W. Balluffi, A quantitative study of vacancy defects in quenched tungsten by combined field-ion microscopy and electrical resistometry, Philos. Mag. A 48 (1983) 397.
[33] M. Yajma, M. Yamagiwa, S. Kajita, N. Ohno, M. Tokitani, A. Takayam, S. Saito, A. M. Ito, H. Nakamura, N. Yoshida, Comparison of damages on tungsten surface exposed to noble gas plasmas, Plasma Sci. Technol. 15 (2013) 282–286.
[34] M. Backman, K.D. Hammond1, F. Sefta, B.D. Wirth, Atomistic simulations of tungsten surface evolution under low-energy neon implantation, Nucl. Fusion 56 (2016) 046008.
[35] G. Kresse, J. Hafner, Ab initio molecular dynamics for liquid metals, Phys. Rev. B 47 (1993) 558.

[36] G. Kresse, J. Furthmuller, Efficient iterative schemes for ab initio total-energy calculations using a plane-wave basis set, Phys. Rev. B 54 (1996) 11169.
[37] J.P. Perdew, K. Burke, M. Ernzerhof, Generalized gradient approximation made simple, Phys. Rev. Lett. 77 (1996) 3865.
[38] J.P. Perdew, J.A. Chevary, S.H. Vosko, K.A. Jackson, M.R. Pederson, D.J. Singh, C. Fiolhais, Atoms, molecules, solids, and surfaces: applications of the generalized gradient approximation for exchange and correlation, Phys. Rev. B 46 (1992) 6671.
[39] J.P. Perdew, J.A. Chevary, S.H. Vosko, K.A. Jackson, M.R. Pederson, D.J. Singh, C. Fiolhais, Erratum: atoms, molecules, solids, and surfaces: applications of the generalized gradient approximation for exchange and correlation, Phys. Rev. B 48 (1993) 4978.
[40] P.E. Blöchl, Projector augmented-wave method, Phys. Rev. B 50 (1994) 17953.
[41] G. Kresse, D. Joubert, From ultrasoft pseudopotentials to the projector augmented-wave method, Phys. Rev. B 59 (1999) 1758.
[42] G.Y. Huang, B.D. Wirth, First-principles study of diffusion of interstitial and vacancy in α U-Zr, J. Phys.: Condens. Matter 23 (2011) 205402.
[43] T. Mattsson, Comparison of PBEsol and AM05, employing two different codes: EMTO-KKR and VASP 5.1 (unpublished), 2008.
[44] J.S. Shah, M.E. Straumanis, Thermal expansion of tungsten at low temperatures, J. Appl. Phys. 42 (1971) 3288.
[45] B.N. Dutta, B. Dayal, Lattice constants and thermal expansion of palladium and tungsten up to 878 °C by X-ray method, Phys. Status Solidi B 3 (1963) 2253.
[46] X.G. Lu, M. Selleby, B. Sundman, Assessments of molar volume and thermal expansion for selected bcc, fcc and hcp metallic elements, Calphad 29 (2005) 68.
[47] J.H. Stathis, D.I. Bolef, Elastic constants of tungsten between 4.2 and 77 K, J. Appl. Phys. 51 (1980) 4770.
[48] N. Soga, Comparison of measured and predicted bulk moduli of tantalum and tungsten at high temperatures, J. Appl. Phys. 37 (1966) 3416.
[49] C. Bercegeay, S. Bernard, First-principles equations of state and elastic properties of seven metals, Phys. Rev. B 72 (2005) 214101.
[50] F.H. Featherston, J.R. Neighbours, Elastic constants of tantalum, tungsten, and molybdenum, Phys. Rev. 130 (1963) 1324.
[51] C.E. Anderson, F.R. Brotzen, Elastic constants of tantalum-tungsten alloys, J. Appl. Phys. 53 (1962) 292.
[52] A.L. Ruoff, C.O. Rodriguez, N.E. Christensen, Elastic moduli of tungsten to 15 Mbar, phase transition at 6.5 Mbar, and rheology to 6 Mbar, Phys. Rev. B 58 (1998) 2998.
[53] D.I. Bolef, J. De Klerk, Elastic constants of single-crystal Mo and W between 77 and 500 K, J. Appl. Phys. 33 (1962) 2311.
[54] K. Maier, M. Peo, B. Saile, H.E. Schaefer, A. Seeger, High-temperature positron annihilation and vacancy formation in refractory metals, Philos. Mag. A 40 (1979) 701.
[55] K.D. Rasch, R.W. Siegel, H. Schultz, Quenching and recovery investigations of vacancies in tungsten, Philos. Mag. A 41 (1980) 91.
[56] L.C. Smedskjaer, G.D. Loper, M.K. Chason, R.W. Siegel, Positron annihilation studies of vacancy formation in tungsten, chromium, and niobium, in: MRS Online Proceeding Library 41, 26–30 NOVEMBER 1984.
[57] J.N. Mundy, Electrical resistivity-temperature scale of tungsten, Philos. Mag. A 46 (1982) 345.
[58] I.M. Neklyudov, E.V. Sadanov, G.D. Tolstolutskaja, V.A. Ksenofontov, T.I. Mazilova, I.M. Mikhailovskij, Interstitial atoms in tungsten: Interaction with free surface and in situ determination of formation energy, Phys. Rev. B 78 (2008) 115418.
[59] R.W. Balluff, Vacancy defect mobilities and binding energies obtained from annealing studies, J. Nucl. Mater. 69 & 70 (1978) 240.
[60] J.N. Mundy, S.T. Ockers, L.C. Smedskjaer, Vacancy migration enthalpy in tungsten at high temperatures, Philos. Mag. A 56 (1987) 851.
[61] C.S. Becquart, C. Domain, U. Sarkar, A. DeBacker, M. Hou, Microstructural evolution of irradiated tungsten: ab initio parameterisation of an OKMC model, J. Nucl. Mater. 403 (2010) 75.
[62] Y.L. Liu, Y. Zhang, H.B. Zhou, G.H. Lu, F. Liu, G.N. Luo, Vacancy trapping mechanism for hydrogen bubble formation in metal, Phys. Rev. B 79 (2009) 172103.
[63] D. Johnson, E. Carter, Hydrogen in tungsten: absorption, diffusion, vacancy trapping, and decohesion, J. Mater. Res. 25 (2010) 315.
[64] S.P. Fitzgerald, D. Nguyen-Manh, Peierls potential for crowdions in the bcc transition metals, Phys. Rev. Lett. 101 (2008) 115504.
[65] M. Backman, N. Juslin, G.Y. Huang, B.D. Wirth, A W-Ne interatomic potential for simulation of neon implantation in tungsten, J. Nucl. Mater. 477 (2016) 37.